CrystEngComm

PAPER

View Article Online
View Journal | View Issue

Cite this: *CrystEngComm*, 2014, **16**, 4546

Received 13th September 2013,
Accepted 11th March 2014

DOI: 10.1039/c3ce41856a

www.rsc.org/crystengcomm

Strengthening N···X halogen bonding *via* nitrogen substitution in the aromatic framework of halogen-substituted arylpyrazinamides†

Hamid Reza Khavasi,* Mahdieh Hosseini, Alireza Azhdari Tehrani and Soheila Naderi

The importance of N···X halogen bonding in a series of *N*-(5-halo-2-pyridinyl)pyrazine-2-carboxamides has been investigated by different methods. The results show that when nitrogen is substituted for carbon in the aryl backbone of the parent compound, it can affect the electron accepting ability of bromine and iodine substituents. Thus, a stronger halogen bond can be formed.

Introduction

Weak non-covalent interactions play an important role in the self-assembly of molecules into supramolecular architectures. Among the non-covalent interactions, halogen bonding (XB) has attracted significant attention due to its potential applications in designing new solids with specific physical and chemical properties.[1] The term halogen bonding describes any non-covalent interaction involving halogens as electrophilic species. The interaction can be schematically described as D···X–Y, where X is the electrophilic halogen atom (XB donor), D is a donor of electron density (XB acceptor), and Y is a carbon, nitrogen or halogen atom.[2] It is well-known that the electron density is anisotropically distributed around the covalently bound halogen atom. As a result, a region with a positive electrostatic potential (the so-called σ-hole) is formed on the outermost portion of the halogen's surface along the direction of the R–X bond, which concomitantly produces a perpendicular belt of negative electrostatic potential around the halogen. The positive character of the σ-hole increases down the group as the size and polarizability of the halogen increase, with a corresponding tendency for a halogen bond to become stronger.[3]

Many attempts have been made to enhance the electrophilicity of halogen atoms by substituting electron withdrawing groups, mostly fluorine[4] atoms and rarely a nitro group,[5] in the vicinity of the halogens. The attachment of a halogen atom to a charged aromatic ring such as pyridinium[6a,b] and pyrimidinium moiety[6c] also has been proposed as an alternative approach to polarize the halogen atom, thereby making it a better halogen bond donor. As part of our research interest in the study of weak intermolecular interactions[7] and also halogen bonded systems,[8] we became interested in exploring how the substitution of nitrogen for carbon in the aryl backbone of halogen-substituted phenylpyrazinamides could change the strength of halogen bonding and therefore affect the supramolecular structure. Thus, in the following, we present the crystal structures of *N*-(5-halo-2-pyridinyl)pyrazine-2-carboxamide, carrying different halogen atoms in the pyridine *para*-position to the amide group. Compounds synthesized here can be schematically shown as **X-py**, where X represents the halogen atom (Scheme 1).

Results and discussion

Synthesis

These compounds were prepared by modification of a method described previously.[8b] Crystals suitable for X-ray analysis were obtained by slow evaporation of methanolic solution at room temperature. For comparing the halogen bonding geometrical parameters of **X-phen** and **X-py**, crystal structures of **X-phen** have been re-determined, at 298 K, here (Table 1 and Fig. S1).†[8b]

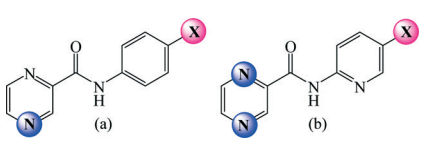

Scheme 1 *N*-(4-halophenyl)pyrazine-2-carboxamide, **X-phen**, structures (a) and *N*-(5-halo-2-pyridinyl)pyrazine-2-carboxamide, **X-py**, structures (b) the halogen bond donor and halogen bond acceptors are shown in purple and blue circles, respectively.

Faculty of Chemistry, Shahid Beheshti University, G. C., Evin, Tehran 1983963113, Iran. E-mail: h-khavasi@sbu.ac.ir; Fax: +98 21 22431663

† Electronic supplementary information (ESI) available: ORTEP diagrams of **X-phen** compounds, electrostatic potentials mapped on the electron isodensity surface of **F-phen**, **Cl-phen**, **F-py** and **Cl-py**, relative contributions of various intermolecular contacts to the Hirshfeld surface area in **F-phen**, **F-py**, **Cl-phen** and **Cl-py** and full crystallographic data. CCDC 951196–951202 and 877918. For ESI and crystallographic data in CIF or other electronic format see DOI: 10.1039/c3ce41856a

Table 1 Structural data and refinement parameters for compounds **F-py**, **Cl-py**, **Br-py**, **I-py**, **F-phen**, **Cl-phen**, **Br-phen** and **I-phen**

	F-py	Cl-py	Br-py	I-py	F-phen	Cl-phen	Br-phen	I-phen
Formula	$C_{10}H_7FN_4O$	$C_{10}H_7ClN_4O$	$C_{10}H_7BrN_4O$	$C_{10}H_7IN_4O$	$C_{11}H_8FN_3O$	$C_{11}H_8ClN_3O$	$C_{11}H_8BrN_3O$	$C_{11}H_8IN_3O$
fw	218.06	234.64	279.09	326.09	217.20	233.65	278.10	325.11
λ/Å, T/K	0.71073, 298(2)	0.71073, 298(2)	0.71073, 298(2)	0.71073, 298(2)	0.71073, 298(2)	0.71073, 298(2)	0.71073, 298(2)	0.71073, 298(2)
Crystal system	Triclinic	Monoclinic	Monoclinic	Monoclinic	Monoclinic, $P2_1/n$	Triclinic	Triclinic	Triclinic
Z, space group	4, $P2_1/n$	4, $P\bar{1}$	8, $P2_1/n$	4, $P2_1/n$	8, $P2_1/c$	2, $P\bar{1}$	2, $P\bar{1}$	2, $P\bar{1}$
a/Å	3.7671(5)	7.375(4)	7.287(2)	5.7717(3)	6.0141(15)	5.8988(19)	5.8743(6)	5.9550(8)
b/Å	15.7465(19)	10.920(5)	24.367(5)	24.9374(8)	23.974(5)	7.408(3)	7.5065(7)	7.7126(11)
c/Å	16.358(2)	13.606(7)	12.004(3)	7.5654(3)	13.582(3)	13.191(4)	13.3959(9)	12.9998(17)
α/°	90	86.20(4)	90	90	90	101.56(3)	101.489(7)	78.850(11)
β/°	92.991(11)	83.56(4)	100.65(2)	94.819(4)	92.58(2)	96.55(2)	96.656(7)	85.640(11)
γ/°	90	73.19(4)	90	90	90	110.55(3)	110.390(8)	70.594(11)
V/Å^3, D_{calc}/g cm^{-3}	969.0(2), 1.496	1041.6(9), 1.496	2094.7(9), 1.770	1085.5(8), 1.996	1956.2(8), 1.475	518.0(3), 1.498	531.44(8), 1.738	552.47(13), 1.954
F(000), 2θ/°	448, 52.00	480, 58.64	1104, 52.00	624, 52.00	896, 58.44	240, 54.00	276, 52.00	312, 58.44
R(int), S	0.0599, 1.002	0.0657, 1.030	0.1256, 0.892	0.2180, 0.910	0.1016, 0.864	0.0998, 1.038	0.0759, 0.998	0.0372, 1.091
R_1, w$R_2(I > 2\sigma(I))$	0.0466, 0.0773	0.0710, 0.1168	0.0812, 0.1605	0.0787, 0.1239	0.0538 0.0885	0.0715, 0.1410	0.0491, 0.1109	0.0296, 0.0668
CCDC no.	951201	951199	951197	951202	951200	951198	951196	877918

Structural analysis of X-py compounds

X-ray crystallographic analyses reveal that **F-py**, **Br-py** and **I-py** crystallize in the monoclinic $P2_1/n$ space group, while **Cl-py** crystallizes in the centrosymmetric triclinic space group $P\bar{1}$. ORTEP diagrams of compounds **X-py** drawn with 30% ellipsoid probability have been shown in Fig. 1. The asymmetric unit of **F-py** consists of one crystallographically independent molecule, $Z' = 1$. In **F-py**, discrete molecules are held together by head-to-tail C_{pyz}–H···N_{py} hydrogen bonds for the generation of a dimeric unit (Fig. 2(a) and Table 2). Adjacent dimeric units are further linked to each other by C_{py}–F···H–C_{pyz} and C_{py}–H···O═C intermolecular interactions in the *bc*-plane. As shown in Fig. 2(b), extensive π–π stacking interactions, in the *a*-direction, also occur when the corresponding molecules are in parallel orientation with respect to one another to form infinite one-dimensional tape (Table 3). Thus, in **F-py**, the overall supramolecular structure is constructed with the cooperation of π···π stacking, hydrogen bonds and C_{pyz}–F···H–C_{pyz} intermolecular interactions.

In **Cl-py** crystal packing, the most noticeable intermolecular features are C═O···H–C_{pyz}, C_{pyz}–H···N_{py} and C_{py}–H···Cl hydrogen bonds (Table 2) that are cooperated with π–π stacking interactions between pyridine and pyrazine rings in the *a*-direction (Fig. 3 and Table 3). Unlike in **Cl-phen**, the chlorine atom in **Cl-py** is not involved in any contacts that can be categorized as halogen bonds. The crystal structure of **Br-py** in the *bc*-plane is built up mainly by two kinds of N···X halogen bonds having different nitrogen atoms as halogen bond acceptors, (C_9–Br_1···N_6 and C_{19}–Br_2···N_1) and N–H···Br and C–H···O═C hydrogen bonds. A view of the crystal structure along the crystallographic *a*-axis reveals that π_{py}···π_{pyz} stacking interactions play an important role in stabilizing the crystal structure (Fig. 4 and Tables 2 and 3). Based on the binding energies obtained from DFT calculations with correction for the basis set superposition error (BSSE), of two

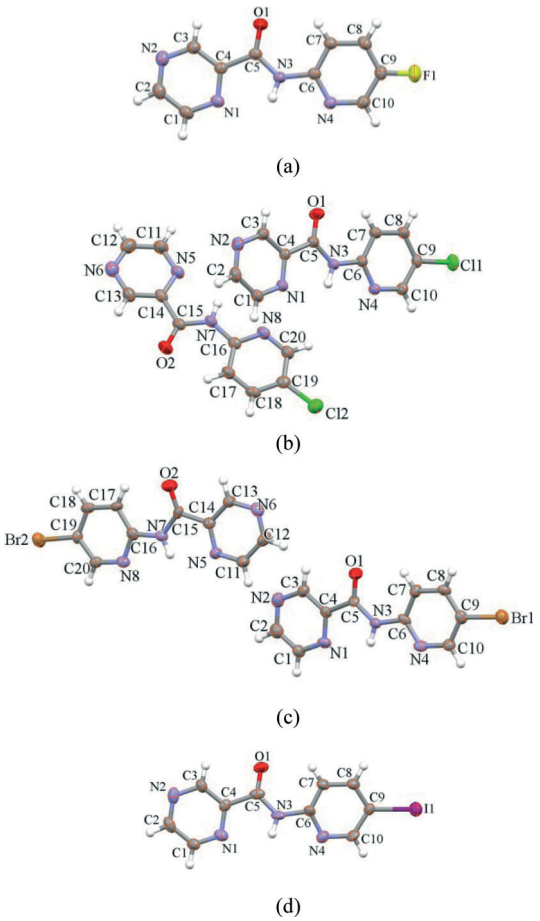

Fig. 1 The ORTEP diagrams of **F-py** (a), **Cl-py** (b), **Br-py** (c) and **I-py** (d) compounds. Ellipsoids are drawn at a 30% probability level.

N···Br halogen bonds, the stronger halogen bond is formed when the pyrazine nitrogen atom, *anti* to the carbonyl, is a

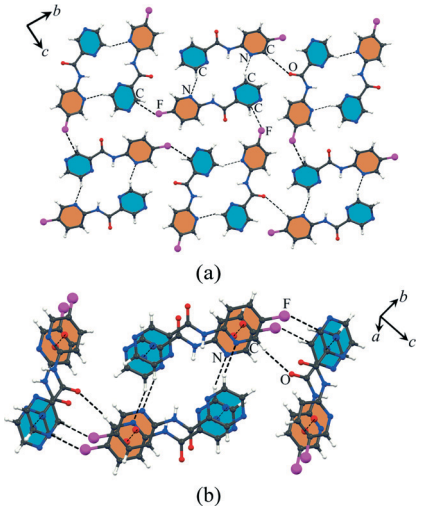

Fig. 2 (a) A side view representation of *N*-(5-fluoro-2-yl)pyrazine-2-carboxamide, **F-py**, in the *bc*-plane, showing the association of the adjacent molecules through head-to-tail C_{pyz}–H···N_{py} hydrogen bonds for the generation of a dimeric unit. Adjacent dimeric units are further linked to each other by C_{py}–F···C_{pyz} and C_{py}–H···O=C intermolecular interactions in the *bc*-plane. (b) A side view representation of **F-py**, showing how extensive π–π stacking interactions, in the *a*-direction, occur when the corresponding molecules are in parallel orientation with respect to one another to form infinite one-dimensional tape.

halogen bond acceptor, of which the C–Br···N angle is farther from 180° but the C–Br···N distance is shorter (Table 4). In the crystal packing of **I-py**, dimeric units are formed alternatively by head-to-tail C_{pyz}–H···N_{py} and C=O···H–C_{py} hydrogen bonds, in the *a*-direction. Adjacent dimeric units are further linked to each other by head-to-tail N···X halogen bonds to generate a wave-like chain (Fig. 5(a)). Extensive $\pi_{py}\cdots\pi_{pyz}$ stacking interactions also stabilize the molecular packing in the *c*-direction (Fig. 5(b) and Table 3).

Strengthening N···X halogen bonding *via* nitrogen substitution in the aromatic framework

A comparison between the significant intermolecular interactions controlling the packing of **X-phen** and **X-py** is illustrated in Scheme 2. A way to understand the strength of XB is considering and analyzing the crystal packing of isomolecular structures. This approach enables systematic investigation of crystal packing changes that arise as a consequence of tuning the relative strength of XB to the other interactions. Here, we report the crystallographic study of an isostructural **X-py** compound, to provide new insights into the understanding of the effect of substituting nitrogen for the CH group in the aromatic backbone of a series of compounds that have been recently investigated by us.[8b] This effect has been studied recently by Blockhuys and his co-workers,[9] who have investigated the factors influencing the activation and de-activation of fluorine synthons, in a different molecular system. The nitrogen atom is isoelectronic with a CH group; thus aromaticity is maintained when CH group(s) constituting the framework of the phenylpyrazinamide system is (are) replaced by the nitrogen atom(s) (Scheme 1). The nitrogen atom of the pyridine ring in the *N*-(5-halo-2-pyridinyl)pyrazine-2-carboxamide molecule imports new features into the crystal engineering of phenylpyrazinamide derivatives. The pyridinic nitrogen atom

Table 2 Selected hydrogen bond geometries for compounds **F-py**, **Cl-py**, **Br-py**, **I-py**, **F-phen**, **Cl-phen**, **Br-phen** and **I-phen**

Compound	D–H···A	*d*(D–H)	*d*(H···A)	*d*(D···A)	<(DHA)
F-py	C10–H10···O1–C5^a	0.93	2.664	3.572(2)	175
	C1–H1···N4$_{py}$^{b}	0.93	2.619	3.495(3)	157
Cl-py	C1–H1···O2–C15^c	0.93	2.483	3.148(4)	129
	C18–H18···O1–C5^d	0.93	2.507	3.391(4)	159
	C2–H2···O2–C15^e	0.93	2.670	3.243(5)	121
	C10–H10···N2$_{pyz}$^{f}	0.93	2.687	3.594(4)	165
	C7–H7···Cl2–C19^g	0.93	2.964	3.689(4)	138
Br-py	C13–H13···O1–C5^h	0.93	2.449	3.26(1)	145
	C7–H7···O2–C15^h	0.93	2.625	3.28(1)	128
	N3–H3B···Br2–C19^a	0.93	2.839	3.681(8)	166
I-py	C8–H8···O1–C5^i	0.93	2.550	3.21(2)	128
	C1–H1···N4$_{py}$^{j}	0.93	2.640	3.54(2)	163
F-phen	C11–H11···O1–C5^k	0.93	2.453	3.293(3)	150
	C13–H13···N2$_{pyz}$^{l}	0.93	2.729	3.581(3)	153
	C19–H19···F1–C9^m	0.93	2.497	3.323(3)	148
	C8–H8···F2–C20^l	0.93	2.609	3.373(3)	140
Cl-phen	C11–H11···O1–C5^k	0.93	2.417	3.21(1)	143
	C1–H1···N2$_{pyz}$^{k}	0.93	2.770	3.59(1)	148
	C3–H3···N1$_{pyz}$^{n}	0.93	2.779	3.61(1)	149
Br-phen	C11–H11···O1–C5^n	0.93	2.469	3.226(7)	139
	C1–H1···N2$_{pyz}$^{n}	0.93	2.764	3.592(8)	149
	C3–H3···N1$_{pyz}$^{o}	0.93	2.774	3.597(7)	148
I-phen	C7–H7···O1–C5^n	0.93	2.398	3.202(4)	145
	C1–H1···N2$_{pyz}$^{n}	0.93	2.841	3.677(5)	150

Symmetry codes:^{a} −1/2 + *x*, 1/2 − *y*, −1/2 + *z*. ^{b} −*x*, 1 − *y*, −*z*. ^{c} 1 − *x*, 1 − *y*, 1 − *z*. ^{d} *x*, *y*, 1 + *z*. ^{e} 1 − *x*, 1 − *y*, 1 − *z*. ^{f} *x*, −1 + *y*, *z*. ^{g} *x*, *y*, −1 + *z*. ^{h} 1 − *x*, −*y*, 3 − *z*. ^{i} −*x*, −*y*, 1 − *z*. ^{j} 2 − *x*, −*y*, 2 − *z*. ^{k} 1 + *x*, *y*, *z*. ^{l} 1 − *x*, −1/2 + *y*, 3/2 − *z*. ^{m} 2 − *x*, 1/2 + *y*, 1.5 − *z*. ^{n} −1 + *x*, *y*, *z*. ^{o} 1 + *x*, *y*, *z*.

Table 3 π–π stacking interaction geometries for compounds **F-py**, **Cl-py**, **Br-py**, **I-py**, **F-phen**, **Cl-phen**, **Br-phen** and **I-phen**

Complex	Interaction	Type of interaction	C–C (Å)	P–P (°)	P–CC (°)
F-py	π–π stacking	π_{pyz}–π_{pyz}, π_{py}–π_{py}	3.767	0.0	25.109, 26.302
Cl-py	π–π stacking	π_{pyz}–π_{py}	3.849, 4.028	3.62	29.551, 28.316, 23.228, 26.252
Br-py	π–π stacking	π_{pyz}–π_{py}	3.727, 3.739, 3.777, 3.805	3.6	19.831, 23.440, 23.877, 22.066
I-py	π–π stacking	π_{pyz}–π_{py}	3.677, 3.977	4.34	22.299, 26.418, 29.306, 33.509
F-phen	π–π stacking	π_{pyz}–π_{phen}	3.764, 3.842, 3.874, 3.785	7.89, 8.37, 8.55, 9.05	25.001, 18.379, 24.577, 18.471 23.454, 21.151, 22.926, 20.572
Cl-phen	π–π stacking	π_{pyz}–π_{phen}	3.865	11.34	16.750, 20.125
	Amide···π	Amide···π	3.494	—	—
Br-phen	π–π stacking	π_{pyz}–π_{phen}	3.904	11.05	19.058, 20.152
	Amide···π	Amide···π	3.534	—	—
I-phen	π–π stacking	π_{pyz}–π_{phen}	3.747, 3.992	8.15	19.180, 13.065, 27.869, 22.429

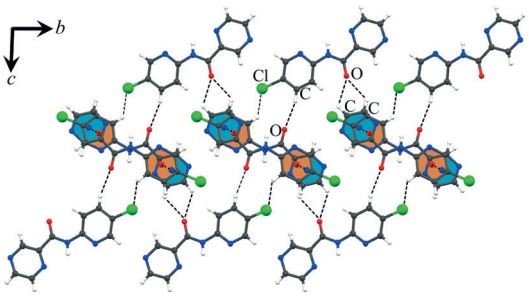

Fig. 3 A side view representation of *N*-(5-chloro-2-yl)pyrazine-2-carboxamide, **Cl-py**, in the *bc*-plane, showing the association of the adjacent molecules through C═O···H–C_{pyz}, C_{pyz}–H···N_{py} and C_{py}–H···Cl hydrogen bonds that are cooperated with π–π stacking interactions between pyridine and pyrazine rings in the *a*-direction.

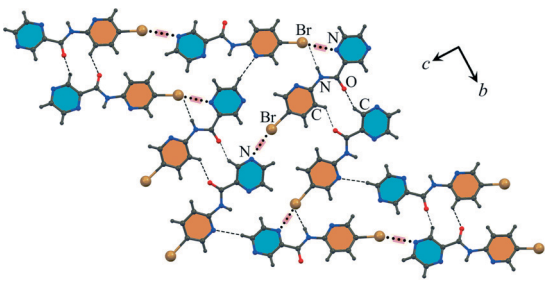

(a)

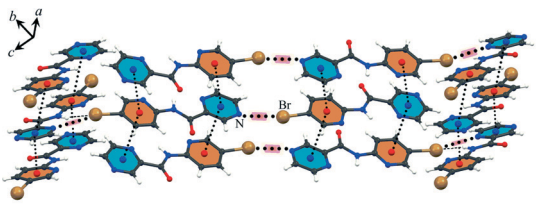

(b)

Fig. 4 (a) A side view representation of *N*-(5-bromo-2-pyridinyl)pyrazine-2-carboxamide, **Br-py**, in the *bc*-plane, showing the formation of a 2D sheet through N···X halogen bonds, and N–H···Br and C–H···O═C hydrogen bonds. (b) A view of the **Br-py** crystal structure along the crystallographic *a*-axis, and the π_{py}···π_{pyz} stacking interactions are in an antiparallel fashion. Halogen bonds are highlighted in red.

either could be directly involved in new intermolecular interactions, such as C–H···N_{py} hydrogen bonds, or could indirectly alter the electron distribution of the aromatic ring, to which the halogen atom is bonded. The dihedral angle between the planes of pyrazine and pyridine rings lies between 1.24 and 4.34° for **X-py** compounds (Table 5). **X-py** compounds, compared with **X-phen**, show better coplanarity between the aromatic rings, which is the consequence of intramolecular N–H···N_{py} hydrogen-bond formation. In addition to intramolecular hydrogen bonding, the pyridinic nitrogen atom is mainly involved in intermolecular C–H···N_{py} hydrogen bonds for the formation of dimeric units (Table 2). Investigations of intermolecular interactions and crystal packing of **F-py** and **Cl-py** *via* Hirshfeld surface analysis[10] reveal that, upon the replacement of the halogen-substituted phenyl group of phenylpyrazinamide by a halogen-substituted pyridine group, the probability of hydrogen bonding increases while that of π···π stacking decreases (Fig. S2).† The differences in the tendency of aromatic rings to stack *via* π-bonding can be elucidated through a comparison of molecular electrostatic potential surfaces of the **F-py** and **Cl-py** as shown in Fig. S3.† The presence of a nitrogen heteroatom within the ring changes the π-electron distribution throughout the carbon backbone, therefore, the aromatic ring in **X-py** becomes considerably electron poorer than in **X-phen**. As a result, the **Cl-py** exhibits crystal packing where hydrogen bonding interactions are favored over weak N···Cl halogen bonding, a type of bonding which has been observed in **Cl-phen** crystal packing. As expected, the halogen bond strength is enhanced by using a heavier halogen substituent. Accordingly, the interesting feature in the crystal structures of **Br-py** and **I-py** is that there is a tendency to form a halogen bonding synthon between halopyridyl and pyrazine rings. For **Br-phen**, **Br-py**, **I-phen** and **I-py**, the N···X distances of 3.284(5), 3.35(1) and 3.26(1), 3.450(3) and 3.11(1) Å, respectively, between halogen and nitrogen atoms are 3.4%, 1.4% and 4.1%, 2.2% and 11.9% shorter than the sum of the van der Waals radii, respectively (Table 4). The θ_{N}···$_{X-C}$ angle of the halogen bonded compounds investigated here varies between 154.0(3)° and 175.9(5)° (Table 4). The nearly linear geometry of N···X is in agreement with the n → σ* character of this

Table 4 Halogen bond geometries and calculated XB binding energies for **Br-phen**, **Br-py**, **I-phen** and **I-py** compounds

Compound	X···N (Å)	C–X···N (°)	Reduction of the sum of the VDW radii (%)	Symmetry code	Calculated XB energy (kJ mol^{-1})
X = Br					
Br-phen	3.284(5)	162.8(2)	3.4	$-1+x, y, -1+z$	−14.03
Br-py	3.35(1)	166.8(4)	1.4	$1-x, -y, 2-z$	−16.63
	3.26(1)	154.0(3)	4.1	$1/2+x, 1/2-y, 1.5+z$	−18.94
X = I					
I-phen	3.450(3)	166.66(9)	2.2	$-1+x, 1+y, -1+z$	−14.52
I-py	3.11(1)	175.9(5)	11.9	$1/2-x, 1/2+y, 1.5-z$	−23.54

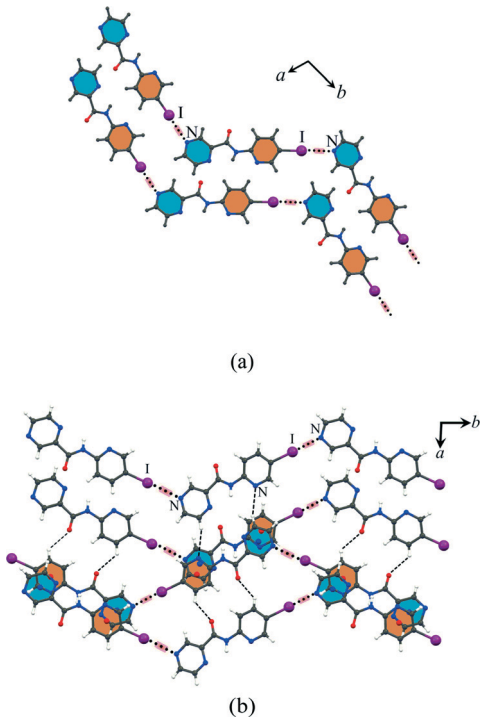

Fig. 5 (a) A side view representation of *N*-(5-iodo-2-pyridinyl)pyrazine-2-carboxamide, **I-py**, in the *ab*-plane, showing the formation of wave-like 1D chains through head-to-tail N···I halogen bonds. (b) Generation of a dimeric unit in **I-py**, by head-to-tail C_{pyz}–H···N_{py} and C=O···H–C_{py} hydrogen bonds, in the *a*-direction. Extensive $\pi_{py}\cdots\pi_{pyz}$ stacking interactions also stabilize the molecular packing in the *c*-direction. Head-to-tail N···I halogen bonds are highlighted in red.

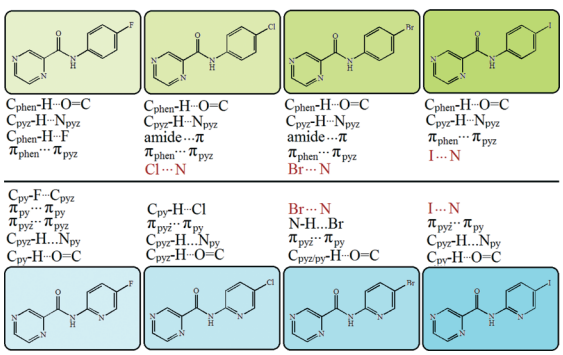

Scheme 2 A comparison between significant intermolecular interactions controlling the packing of **X-phen** and **X-py**.

Table 5 Dihedral angles between plane *A*, plane *B* and the amide plane in **X-phen** and **X-py** compounds (plane *A* = pyrazine ring, plane *B* = phenyl or pyridyl ring)

Compound	∠Amide plane and plane *A* (°)	∠Amide plane and plane *B* (°)	∠Plane *A* and plane *A* (°)
F-py	3.45	2.13	1.24
Cl-py	2.62, 6.53	3.97, 2.93	3.26, 3.62
Br-py	5.60, 2.31	3.35, 1.70	3.52, 3.95
I-py	8.15	12.44	4.34
F-phen	4.17, 5.11	12.030, 14.16	7.89, 9.05
Cl-phen	0.52	11.38	11.34
Br-phen	0.96	12.00	11.05
I-phen	3.08	11.00	8.15
Definition of geometrical parameters	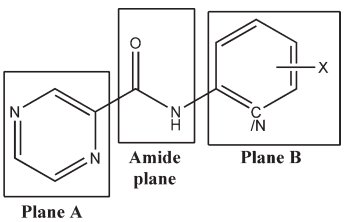		

bonding interaction.[1b,c] The stronger participation of the bromine atom in **Br-py**, compared with **Br-phen**, suggests that the pyridinic nitrogen exerts a polarizing effect on the halogen atom, thereby promoting larger σ-hole (Fig. 6). This has been manifested in the higher proportion of halogen bonding interactions in **Br-py** (6.1%) relative to **Br-phen** (4.6%) (Fig. 7). In the case of **I-py**, the pyridinic nitrogen atom induces a stronger polarizing effect on the halogen substituent, due to the higher polarizability of the iodine atom. Thus, the participation of iodine in N···X halogen bonding is approximately doubled from **I-phen** (3.1%) to **I-py** (6.0%).

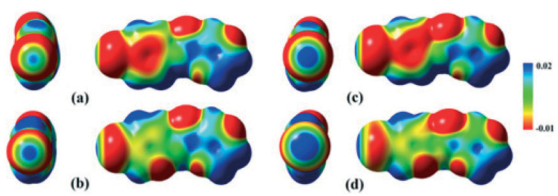

Fig. 6 Electrostatic potentials mapped on the electron isodensity surface of **Br-phen** (a) **Br-py** (b) **I-phen** (c) and **I-py** (d) at the same contour value of 0.001 electron per Bohr^3. The red color shows the most negative potential, while the blue color represents the most positive one. The side view representation of the halogen σ-hole is shown on the left side of each MEP.

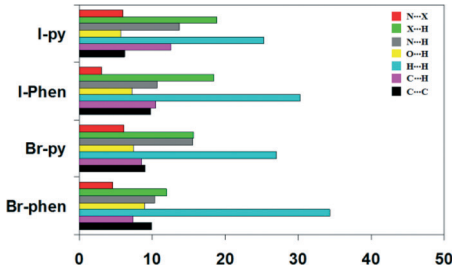

Fig. 7 Relative contributions of various intermolecular contacts to the Hirshfeld surface area in **Br-phen**, **Br-py**, **I-phen** and **I-py** compounds.

It was of interest to investigate further, using theoretical methods, the halogen bonding energy in **Br-phen**, **Br-py**, **I-phen** and **I-py** compounds. The binding energies obtained from DFT calculation with correction for the basis set superposition error (BSSE) on two relative fragments provide us an opportunity to evaluate the halogen bonding interaction energy between two fragments. The selected fragments were cut out directly from CIF data. The outcomes obtained from DFT methods are listed in Table 4. From these data, it is shown that N···X (X = Br and I) halogen bonding energies vary within a range of −14.03 to −23.54 kJ mol^{-1}. The theoretical results show that the halogen bonding interaction energy increases from **Br-phen to Br-py** and from **I-phen to I-py** (Table 4). Interestingly enough, in the **X-phen** (X = Cl, Br, I) and **X-py** (X = Br, I) series, the melting points are increased by increasing the strength of halogen bonding interaction energies.

Conclusion

In conclusion, replacement of CH groups in **Br-phen** and **I-phen** compounds with nitrogen atoms leads to crystal structures where the importance of halogen bonding becomes even more pronounced. Interestingly enough, in the **X-phen** (X = Cl, Br, I) and **X-py** (X = Br, I) series, the melting points are increased by increasing the strength of halogen bonding interaction energies. The results of this study should provide an additional design tool in crystal engineering to tune the relative strength of the halogen bonding.

Experimental section

Chemicals and instrumentation

All solvents such as methanol and pyridine and the chemicals were commercially available (reagent grade) and were purchased from Merck and Aldrich and used without further purification. Infrared spectra (4000–400 cm^{-1}) of the solid samples were taken as 1% dispersion in KBr pellets using a BOMEM-MB102 spectrometer. ^{1}H NMR spectra were recorded using a Bruker AC-300 MHz spectrometer at ambient temperature in CD_3OD. All chemical shifts are quoted in parts per million (ppm) relative to tetramethylsilane. The melting point was obtained using a Bamstead Electrothermal type 9200 melting point apparatus and corrected.

Synthesis of *N*-(5-halophenyl)-2-pyrazinecarboxamides, X-phen

The compounds **F-phen**, **Cl-phen**, **Br-phen** and **I-phen** were prepared by simply mixing the same equivalents of *para*-haloaniline and pyrazinecarboxylic acid in pyridine in the presence of triphenyl phosphate, according to what has been reported previously.[8b]

Synthesis of *N*-(5-fluoro-2-yl)pyrazine-2-carboxamide, F-py

The *N*-(5-fluoro-2-yl)pyrazine-2-carboxamide compounds were prepared by the reaction of 2-amino-5-fluoropyridine (5 mmol) and pyrazine-2-carboxylic acid (5 mmol) in pyridine at boiling point temperature and under reflux conditions. Specifically, 2-amino-5-fluoropyridine (5 mmol) in 15 ml pyridine was added to a solution of pyrazine-2-carboxylic acid (5 mmol) in 15 ml pyridine. The resulting solution was stirred at 313 K for 20 min, then triphenyl phosphite (5 mmol) was added dropwise, and the reaction mixture was stirred for 5 h at 373 K and for 24 h at ambient temperature. The mixture was added to 200 ml distilled water. Precipitation of a white solid resulted in a yield of 60%, which was filtered off and dried under reduced pressure. Upon slow evaporation of the filtrate at room temperature, suitable crystals of **F-py** for X-ray analysis were obtained after 6 days (melting point = 161 °C). Anal. calcd for $C_{10}H_7FN_4O$: C, 55.05; H, 3.23; N, 25.68. Found: C, 54.85; H, 3.14; N, 25.48. FT-IR (KBr pellet, cm^{-1}): 3339, 1944, 1844, 1696, 1577, 1543, 1398, 1229, 1102, 1014, 841, 769, 674, 534, 423. ^{1}H NMR ($CDCl_3$, δ from TMS): 10.21 (1H-pyrazine), 9.50 (amidic H), 8.83 (1H-pyrazine), 8.62 (1H-pyrazine), 8.42–8.46 (1H-pyridine), 8.22 (1H-pyridine) and 7.49–7.55 (1H-pyridine).

Synthesis of *N*-(5-chloro-2-yl)pyrazine-2-carboxamide, Cl-py

The procedure was similar to the synthesis of **F-py** except that 2-amino-5-chloropyridine was used instead of 2-amino-5-fluoropyridine. Precipitation of a white solid resulted in a yield of 70%, which was filtered off and dried under reduced pressure. Upon slow evaporation of the filtrate at room temperature, suitable crystals of **Cl-py** for X-ray analysis were obtained after 7 days (melting point = 165 °C). Anal. calcd for $C_{10}H_7ClN_4O$: C, 51.19; H, 3.01; N, 23.88. Found: C, 51.15; H, 2.95; N, 23.76. FT-IR (KBr pellet, cm^{-1}): 3352, 1957, 1698, 1572, 1523, 1462, 1380, 1301, 1100, 1016, 842, 736, 680, 438, 302. ^{1}H NMR ($CDCl_3$, δ from TMS): 10.23 (1H-pyrazine), 9.51 (amidic H), 8.84 (1H-pyrazine), 8.63 (1H-pyrazine), 840–8.43 (1H-pyridine), 8.33 (1H-pyridine), 7.74–7.78 (1H-pyridine).

Synthesis of *N*-(5-bromo-2-yl)pyrazine-2-carboxamide, Br-py

The procedure was similar to the synthesis of **F-py** except that 2-amino-5-bromopyridine was used instead of 2-amino-5-fluoropyridine. Precipitation of a white solid resulted in a yield of 55%, which was filtered off and dried under reduced pressure. Upon slow evaporation of the filtrate at room temperature, suitable crystals of **Br-py** for X-ray analysis were obtained after 8 days (melting point = 166 °C).

Anal. calcd for $C_{10}H_7BrN_4O$: C, 43.03; H, 2.53; N, 20.07. Found: C, 42.97; H, 2.45; N, 19.72. FT-IR (KBr pellet, cm^{-1}): 3339, 1900, 1823, 1700, 1570, 1525, 1356, 1283, 1087, 1035, 829, 776, 663, 502, 438. ^1H NMR ($CDCl_3$, δ from TMS): 10.22 (1H-pyrazine), 9.51 (amidic H), 8.84 (1H-pyrazine), 8.63 (1H-pyrazine), 8.50–8.53 (1H-pyridine), 8.35–8.42 (1H-pyridine) and 7.87–7.9 (1H-pyridine).

Synthesis of *N*-(5-iodo-2-yl)pyrazine-2-carboxamide, I-py

The procedure was similar to the synthesis of **F-py** except that 2-amino-5-iodopyridine was used instead of 2-amino-5-fluoropyridine. Precipitation of a white solid resulted in a yield of 70%, which was filtered off and dried under reduced pressure. Upon slow evaporation of the filtrate at room temperature, suitable crystals of **I-py** for X-ray analysis were obtained after 8 days (melting point = 170 °C). Anal. calcd for $C_{10}H_7IN_4O$: C, 36.83; H, 2.16; N, 17.18. Found: C, 36.80; H, 2.14; N, 17.13. FT-IR (KBr pellet, cm^{-1}): 3352, 1690, 1563, 1530, 1356, 1290, 989, 842, 660, 522, 441, 275. ^1H NMR ($CDCl_3$, δ from TMS): 10.18 (1H-pyrazine), 9.49 (amidic H), 8.83 (1H-pyrazine), 8.62 (1H-pyrazine), 8.55 (1H-pyridine), 8.24–8.27 (1H-pyridine) and 8.02–8.05 (1H-pyridine).

Single crystal diffraction studies

For all compounds apart from F-phen, the intensity data were collected using STOE IPDS-II or STOE-IPDS-2 T diffractometers with graphite monochromated Mo-Kα radiation, 0.71073 Å. Data were collected at a temperature of 298(2) K in a series of ω scans in 1° oscillations and integrated using the Stoe X-AREA[11] software package. A numerical absorption correction was applied using the X-RED[12] and X-SHAPE[13] software. The X-ray data for compound F-phen were collected using a Bruker SMART APEX-II CCD diffractometer equipped with fine focus 1.75 kW sealed tube Mo-Kα radiation, 0.71073 (Å). The total number of images was based on the results from the program COSMO.[14] Cell parameters were retrieved using the APEX II software[15] and refined using SAINT on all observed reflections. Data reduction was performed using the SAINT software,[16] which corrects for Lorentz and Polarizing effects. Scaling and absorption corrections were applied using the SADABS[17] multi-scan technique, supplied by George Sheldrick. All of the structures were solved by direct methods using SHELXS-97 and refined with full-matrix least-squares on F^2 using the SHELXL-97 program package.[18] All non-hydrogen atoms were refined anisotropically. Hydrogen atoms were added at ideal positions and constrained to ride on their parent atoms, with $U_{iso}(H) = 1.2\ U_{eq}$. All of the refinements were performed using the X-STEP32 crystallographic software package.[19] Structural illustrations have been drawn using the MERCURY[20] windows. ORTEP diagrams of these complexes are shown in Fig. 1 and S1.† Crystallographic details including crystal data and structure refinement parameters are listed in Table S1.†

Computational details

DFT calculations were performed using the ORCA quantum chemistry suite.[21] The local spin density approximation (LSD) exchange correlation potential was used with the local density approximation of the correlation energy.[22] Gradient-corrected geometry optimizations[23] were performed by using the generalized gradient approximation (Perdew–Wang non-local exchange and correlation corrections-PW91).[24] The selected two fragments were cut out directly from the CIF data without optimization. Large atom basis sets TZP are used to ascribe all the atoms here. A frozen core approximation was used to treat the core electrons: (1s) for C and N, (4p) for I, (3p) for Br, (2p) for Cl, (1s) for O and F. Scalar relativistic effects were taken into account by using the zeroth-order regular approximation (ZORA).[25]

Computational details for generating molecular electrostatic potential surfaces

Electrostatic potential surfaces were generated for **F-phen**, **F-py**, **Cl-phen**, **Cl-py**, **Br-phen**, **Br-py**, **I-phen** and **I-py** from DFT calculations performed at the B3LYP/6-311G (d,p) basis set level for all atoms except iodine, and the LANL2DZdp-ECP (with polarization functions of d symmetry and diffuse functions of p symmetry) basis set level for iodine. Potential surfaces were mapped by conventional molecular electron density (0.001 electron per $Bohr^3$) and color-coding.

Acknowledgements

We would like to thank the Graduate Study Councils of Shahid Beheshti University, General Campus, and the Iran National Elite Foundation for financial support.

Notes and references

1 (*a*) P. Metrangolo and G. Resnati, *Cryst. Growth Des.*, 2012, **12**, 5835–5838; (*b*) W. T. Pennington, G. Resnati and M. S. Taylor, *CrystEngComm*, 2013, **15**, 3057–3057; (*c*) G. Metrangolo and G. Resnati, *Halogen Bonding: Fundamentals and Applications*, Springer, Berlin, 2008; (*d*) L. Meazza, J. Martí-Rujas, G. Terraneo, C. Castiglioni, A. Milani, T. Pilati, P. Metrangolo and G. Resnati, *CrystEngComm*, 2011, **13**, 4427–4435; (*e*) K. Raatikainen and K. Rissanen, *Chem. Sci.*, 2012, **3**, 1235; (*f*) J. Martí-Rujas, L. Colombo, J. Lü, A. Dey, G. Terraneo, P. Metrangolo, T. Pilati and G. Resnati, *Chem. Commun.*, 2012, **48**, 8207–8209; (*g*) J. Martí-Rujas, L. Meazza, G. Keat Lim, G. Terraneo, T. Pilati, K. D. M. Harris, P. Metrangolo and G. Resnati, *Angew. Chem., Int. Ed.*, 2013, **52**, 13444–13448.

2 (*a*) P. Metrangolo, H. Neukirch, T. Pilati and G. Resnati, *Acc. Chem. Res.*, 2005, **38**, 386–395; (*b*) P. Metrangolo, F. Meyer, T. Pilati, G. Resnati and G. Terraneo, *Angew. Chem., Int. Ed.*, 2008, **47**, 6114–6121.

3 P. Politzer and J. S. Murray, *ChemPhysChem*, 2013, **14**, 278.

4 (*a*) L. C. Roper, C. Präsang, V. N. Kozhevnikov, A. C. Whitwood, P. B. Karadakov and D. W. Bruce, *Cryst. Growth Des.*, 2010,

10, 3710–3720; (*b*) C. Präsang, A. C. Whitwood and D. W. Bruce, *Cryst. Growth Des.*, 2009, **9**, 5319–5326; (*c*) G. Valerio, G. Raos, S. V. Mielle, P. Metrangolo and G. Resnati, *J. Phys. Chem. A*, 2000, **104**, 1617–1620.

5 (*a*) K. Raatikainen and K. Rissanen, *CrystEngComm*, 2009, **11**, 750–752; (*b*) S. J. Garden, F. R. da Cunha, J. L. Wardell, J. M. S. Skakle, J. N. Low and C. Glidewell, *Acta Crystallogr., Sect. C: Cryst. Struct. Commun.*, 2002, **58**, 463–465.

6 (*a*) T. A. Logothetis, F. Meyer, P. Metrangolo, T. Pilati and G. Resnati, *New J. Chem.*, 2004, **28**, 760–763; (*b*) K. Raatikainen, M. Cametti and K. Rissanen, *Beilstein J. Org. Chem.*, 2010, **6**, 4; (*c*) K. E. Riley, J. S. Murray, P. Politzer, M. C. Concha and P. Hobza, *J. Chem. Theory Comput.*, 2009, **5**, 155.

7 (*a*) H. R. Khavasi and B. Mir Mohammad Sadegh, *Cryst. Growth Des.*, 2012, **12**, 4798–4804; (*b*) H. R. Khavasi and M. Azizpoor Fard, *Cryst. Growth Des.*, 2010, **10**, 1892–1896; (*c*) H. R. Khavasi, A. R. Salimi, H. Eshtiagh-Hosseini and M. M. Amini, *CrystEngComm*, 2011, **13**, 3710–3717.

8 (*a*) H. R. Khavasi and A. Azhdari Tehrani, *Inorg. Chem.*, 2013, **52**, 2891–2905; (*b*) H. R. Khavasi and A. Azhdari Tehrani, *CrystEngComm*, 2013, **15**, 3222–3235.

9 A. Collas, R. De Borger, T. Amanova and F. Blockhuys, *CrystEngComm*, 2011, **13**, 702–710.

10 (*a*) J. J. McKinnon, M. A. Spackman and A. S. Mitchell, *Acta Crystallogr., Sect. B: Struct. Sci.*, 2004, **60**, 627–668; (*b*) M. A. Spackman and J. J. McKinnon, *CrystEngComm*, 2002, **4**, 378–392; (*c*) S. K. Wolff, D. J. Grimwood, J. J. McKinnon, M. J. Turner, D. Jayatilaka and M. A. Spackman, *CrystalExplorer 3.0*, University of Western Australia, Perth, Australia, 2012.

11 *X-AREA, version 1.30, program for the acquisition and analysis of data*, Stoe & Cie GmbH, Darmatadt, Germany, 2005.

12 *X-RED, version 1.28b, program for data reduction and absorption correction*, Stoe & Cie GmbH, Darmatadt, Germany, 2005.

13 *X-SHAPE, version 2.05, program for crystal optimization for numerical absorption correction*, Stoe & Cie GmbH, Darmatadt, Germany, 2004.

14 *COSMO V1.58, Software for the CCD Detector Systems for Determining Data Collection Parameters*, Bruker Analytical X-ray Systems, Madison, WI, 2008.

15 *APEX2 V2008.5-0 Software for the CCD Detector System*, Bruker Analytical X-ray Systems, Madison, WI, 2008.

16 *SAINT V 7.34 Software for the Integration of CCD Detector System* Bruker Analytical X-ray Systems, Madison, WI, 2008.

17 *SADABS V2.008/2 Program for absorption corrections using Bruker-AXS CCD based on the method of Robert Blessing*; R. H. Blessing, *Acta Crystallogr., Sect. A: Found. Crystallogr.*, 1995, **51**, 33–38.

18 G. M. Sheldrick, *SHELX97, program for crystal structure solution and refinement*, University of Göttingen, Göttingen, Germany, 1997.

19 *X-STEP32, version 1.07b, crystallographic package*, Stoe & Cie GmbH, Darmstadt, Germany, 2000.

20 *Mercury 3.1 Supplied with Cambridge Structural Database*, CCDC, Cambridge, U.K., 2003–2004.

21 F. Neese, U. Becker, D. Ganyushin, D. G. Liakos, S. Kossmann, T. Petrenko, C. Riplinger and F. Wennmohs, *ORCA, 2.7.0*, University of Bonn, Bonn, 2009.

22 S. H. Vosko, L. Wilk and M. Nusair, *Can. J. Phys.*, 1980, **58**, 1200.

23 (*a*) L. Versluis and T. Ziegler, *J. Chem. Phys.*, 1988, **88**, 322; (*b*) L. Fan and T. Ziegler, *J. Chem. Phys.*, 1991, **95**, 7401.

24 J. P. Perdew, J. A. Chevary, S. H. Vosko, K. A. Jackson, M. R. Pederson, D. J. Singh and C. Fiolhais, *Phys. Rev. D: Part. Fields*, 1992, **46**, 6671.

25 (*a*) E. van Lenthe, E. J. Baerends and J. G. Snijders, *J. Chem. Phys.*, 1993, **99**, 4597; (*b*) E. van Lenthe, E. J. Baerends and J. G. Snijders, *J. Chem. Phys.*, 1994, **101**, 9783; (*c*) E. van Lenthe, R. van Leeuwen, E. J. Baerends and J. G. Snijders, *Int. J. Quantum Chem.*, 1996, **57**, 281.